Ion-Exchange Properties of Microporous Tungstates

Christopher S. Griffith and Vittorio Luca*

Australian Nuclear Science and Technology Organization, PMB 1, Menai, NSW 2234, Australia

Received April 26, 2004. Revised Manuscript Received July 23, 2004

Hydrothermally prepared microporous, hexagonal tungsten bronze (HTB) phases display promising distribution coefficients (K_d) for both Cs^+ (2−100 ppm) and Sr^{2+} (0.5−60 ppm) cations in acidic (1.0 M HNO_3) radioactive waste (radwaste) simulants. The selectivity for Cs^+ and Sr^{2+} increases significantly on isomorphous substitution of molybdenum into the tungstate framework and is optimal for material of composition $Na_{0.2}Mo_{0.03}W_{0.97}O_3{\cdot}ZH_2O$. This composition results from attempts to prepare materials doped at a 10 atom % level viz. $Na_{0.2}Mo_{0.1}W_{0.9}O_3{\cdot}ZH_2O$ ($Mo_{0.1}$−HTB). Both the parent HTB and $Mo_{0.1}$−HTB phases reach maximum uptake of Cs^+ and Sr^{2+} after 30−60 min contact. The cation exchange capacity (CEC) of the parent HTB phase for Cs^+ and Sr^{2+} is ca. 0.2 mmol·g^{-1} (26.6 g·kg^{-1}) and 0.12 mmol·g^{-1} (10.5 g·kg^{-1}), respectively, with a 100% increase displayed on 0.03 atom % molybdenum incorporation into the tungstate framework. The optimized $Mo_{0.1}$−HTB sorbent displays good tolerance of the alkali metal cations, Na^+, K^+, and Ca^{2+}, with respect to the sorption of Cs^+ from acidic solutions. In contrast, the sorption of Sr^{2+} from similar solutions is reduced to a much greater extent by the presence of these cations.

Introduction

A significant problem faced by the nuclear industry is the treatment of radioactive waste generated by weapons production, nuclear fuel recycling, and medical isotope generation. A commonly proposed strategy for dealing with older radioactive liquid waste involves separation of isotopes such as ^{137}Cs and ^{90}Sr from the fission product soup since these are responsible for most of the radioactivity. Ion-exchange using inorganic materials is one intensively investigated method for performing this separation. The strategy of pretreatment using ion-exchange concentrates the radioactivity onto a small volume of sorbent, thus allowing the bulk of the effluent to be disposed as low-level waste with concomitant cost savings.[1] Inorganic ion-exchangers are preferred over organic systems because they are generally regarded to have superior selectivity and radiation stability.[2] A wide range of other materials has been investigated for this application over the past decade, but none effectively sorb both Cs^+ and Sr^{2+} from acidic solutions. Of the most considered materials that show selectivity for Cs^+ in acid solutions, the ammonium molybdophosphates[3] and crystalline silicotitanate (CST) have questionable stability, especially at elevated temperature.[4] Others, such as the hexacyanoferrates, are subject to interference by species such as Hg^{2+} which is present in some acidic radioactive wastes. On the other hand, materials that display selectivity for Sr^{2+} in highly acidic solutions, such as antimonic acids, are generally not selective for Cs^+ and often display unexceptional cation exchange capacity (CEC).[5−11] Encouraging results with antimony-based pyrochlores were reported recently by Moller et al.[10]; however, the acidic solutions had a concentration of only 0.1 mol/L, and Cs^+ and Sr^{2+} were present at only tracer level. Thus, materials that are selective for both cations in strongly acidic media do not yet appear to exist. The advantage of multiple adsorption on a single material is simplicity in disposing of the material once it is saturated since only a single waste stream is produced.

A common structural feature of many inorganic ion-exchangers (Cs^+ or Sr^{2+} selective) is the presence of structural channels, the dimensionality of which is undoubtedly at least partially responsible for their high Cs^+ or Sr^{2+} selectivity.[12]

Tungsten oxides with the hexagonal tungsten bronze structure were first prepared more than five decades ago. Magneli[13] described the structure of the M_xWO_3 hexagonal tungsten bronzes where M = K^+, Rb^+, and Cs^+ prepared by heating mixtures of WO_3 with K, Rb, or Cs tungstates in reducing atmospheres. Other tung-

* To whom correspondence should be addressed. E-mail: vlu@ansto.gov.au. Tel: 61-2-9717 3087. Fax: 61-2-9543 7179.

(1) Todd, T. A.; Brewer, K. N.; Law, J. D.; Wood, D. J.; Garn, T. G.; Tillotson, R. D.; Tullock, P. A.; Wade, E. L. *Waste Manage.* **1997**, 2368−2376.
(2) Sebesta, F. *NATO Sci. Ser., Ser. E* **1999**, *362*, 473.
(3) Miller, C. J.; Olson, A. L.; Johnson, C. K. *Sep. Sci. Technol.* **1997**, *32*, 37.
(4) Taylor, P. A.; Mattus, C. H. *Thermal and Chemical Stability of Silicotitanate Sorbent*; ORNL/TM-2000/307; U.S. Government Printing Office: Washington, DC, 2001.
(5) Baetsle, L. H.; Huys, D. *J. Inorg. Nucl. Chem.* **1968**, *30*, 639.
(6) Moller, T.; Harjula, R.; Kelokaski, P.; Vaaramaa, K.; Karhu, P.; Lehto, J. *J. Mater. Chem.* **2003**, *13*, 535.
(7) Lehto, J.; Harjula, R. *Radiochim. Acta* **1999**, *86*, 65.
(8) Moller, T.; Clearfield, A.; Harjula, R. *Chem. Mater.* **2001**, *13*, 4767.
(9) Karhu, P.; Moller, T.; Harjula, R.; Lehto, J. *Ion Exchange at the Millennium, Proceedings of IEX 2000, 8th, Cambridge, United Kingdom, July 16−21, 2000;* pp 109−115.
(10) Moller, T.; Harjula, R.; Pillinger, M.; Dyer, A.; Newton, J.; Tusa, E.; Amin, S.; Webb, M.; Araya, A. *J. Mater. Chem.* **2001**, *11*, 1526.
(11) Moller, T.; Clearfield, A.; Harjula, R. *Microporous Mesoporous Mater.* **2002**, *54*, 187.
(12) Clearfield, A. *Solvent Extr. Ion Exch.* **2000**, *18*, 655.
(13) Magneli, A. *Acta Chem. Scand.* **1953**, *7*, 315.

10.1021/cm049335w CCC: $27.50
Published on Web 10/23/2004

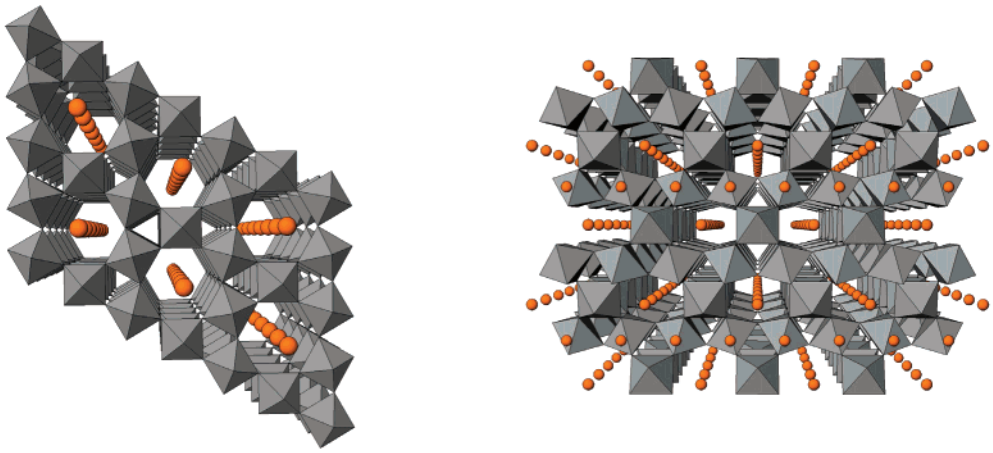

Figure 1. Microporous tungsten oxide phases hexagonal tungsten bronze (HTB) (left) and pyrochlore (PYRO) (right), as viewed down the *c*-axes.

sten bronze compounds with formula M_xWO_3 have also traditionally been prepared by high-temperature methods in reducing environments. For such high-temperature materials, charge compensation is due to pentavalent tungsten atoms and therefore the general formula could be written as $M_xW^{6-x}O_3$. The type of structure that is formed is dependent on the cation that occupies the tunnel positions so that, in general, small cations (e.g., La^{3+}, Ce^{4+}) favor formation of cubic bronzes, intermediate-sized cations (e.g., Na^+) favor formation of tetragonal bronzes, and large-tunnel cations (e.g., K^+, Rb^+, Cs^+, Ba^{2+}) favor formation of hexagonal structures. It is also possible that a single-tunnel cation can give rise to different structures depending on the value of x in the formula. These high-temperature bronze materials have negligible ion exchange capacity and cannot be hydrated.

Gerand et al.[14] were the first to synthesize hydrous tungsten trioxide compounds with a hexagonal tungsten bronze-like structure through wet chemical methods. The compound they synthesized also possessed hexagonal tunnels and a structure very similar to high-temperature hexagonal tungsten bronze compounds but with orthorhombic symmetry and containing structural water molecules as indicated by the formula $WO_3 \cdot {}^1/_3H_2O$. Related compounds were later described by Figlarz[15] who also discussed thermally driven structural transformations in empty-tunnel orthorhombic $Mo_xW_{1-x}O_3$ compounds. Kudo et al.[16] were the first to prepare HTB compounds from peroxo-polytungstate solutions.

The synthesis of hexagonal, pyrochlore, and perovskite tungsten oxides containing Na^+ cations in tunnel sites can be achieved by adjusting the pH of a sodium tungstate solution followed by hydrothermal treatment at low temperatures (140−200 °C), and this was first demonstrated by Reis et al.[17−19] These hydrated microcrystalline materials have a pale yellow-green color and the tungsten valence is predominantly hexavalent. The charge compensation mechanism in these systems is presumed to be due to oxygen atoms present in the tunnel sites and therefore the formula may be given as $M_xWO_{3+x/2} \cdot ZH_2O$. Oxygen atoms present in tunnel sites are presumed to diffuse in and out of the tunnels as the material is oxidized and reduced.

The structures of these microcrystalline bronze materials with formula $Na_xWO_{3+x/2} \cdot ZH_2O$ have been analyzed using Rietveld techniques.[20] The structure was refined in space group *P*6/*mmm* and was reported to be similar to that of high-temperature-reduced HTB except that it contains Na^+ ions at (0, 0, 0) together with water molecules along the hexagonal tunnel at position with the oxygen at (0, 0, 0.4) (Figure 1). In the case of the pyrochlore (PYRO) materials prepared under similar conditions, their structures also possess hexagonal channels. Antimonic acids which have been mentioned above in fact also have this defect pyrochlore structure. Both the HTB and PYRO systems contain water molecules, oxygen anions, and/or hydroxyl groups within the tunnel positions in addition to exchangeable cations. Extant investigations of the HTB phase have shown that the Na^+ cations initially present within the structural tunnels can be completely replaced by other alkali metal cations such as Cs^+, K^+, and Rb^+ by ion-exchange using concentrated solutions.[19] Surprisingly, however, the ion-exchange properties of these microporous HTB materials have been relatively little studied.

We have recently discovered that such compounds have exceptional stability in highly acidic solutions and high selectivities for cations such as Cs^+, Sr^{2+}, Ag^+, Pb^{2+}, and Po^{4+}. This paper addresses the Cs^+ and Sr^{2+} selectivity of HTB materials, in particular, as it relates to the separation of ^{137}Cs and ^{90}Sr from acidic radwaste. In addition, we report on initial attempts to improve the ion-exchange properties by incorporating hetero-elements such as molybdenum into the tungstate framework.

Experimental Section

Standard laboratory grade reagents (>98% purity) from Sigma Aldrich were employed for all syntheses and ion-

(14) Gerand, B.; Nowogrocki, G.; Guenot, J.; Figlarz, M. *J. Solid State Chem.* **1979**, *29*, 429.
(15) Figlarz, M. *Chem. Scr.* **1988**, *28*, 3.
(16) Kudo, T.; Kishimoto, A.; Oi, J.; Inoue, H. *Solid State Ionics* **1990**, *40*−*41*, 567.
(17) Reis, K. P.; Ramanan, A.; Gloffke, W.; Whittingham, M. S. *Mater. Res. Soc. Symp. Proc.* **1991**, *210*, 473.
(18) Reis, K. P.; Ramanan, A.; Whittingham, M. S. *Chem. Mater.* **1990**, *2*, 219.
(19) Reis, K. P.; Ramanan, A.; Whittingham, M. S. *J. Solid State Chem.* **1992**, *96*, 31.
(20) Reis, K. P.; Prince, E.; Whittingham, M. S. *Chem. Mater.* **1992**, *4*, 307.

exchange investigations. The composite absorber, ammonium molybdophosphate/polyacrylonitrile (AMP/PANsf, 85.7% w/w, 0.3−0.63 mm bead size), was kindly supplied by Professor Ferdinand Sebesta, Czech Technical University in Prague. The undoped and Nb-doped silicotitanate materials, $Na_2Ti_{2-x}Nb_xO_3SiO_4 \cdot 2H_2O$ ($x = 0$, 0.1, 0.2, and 0.3),[21,22] and the antimony silicates, $A_xSi_ySb_{6-y}O_6OH$ ($y = 0$, 0.3, and 0.6),[10] with pyrochlore symmetry were prepared as described previously.

Synthesis of $Na_{0.2}Mo_yW_{1-y}O_3 \cdot ZH_2O$ ($y = 0-0.2$). The hexagonal tungsten bronze (HTB, $y = 0$) phase was prepared according to the methodology of Reis and co-workers[18,19] in which Na_2WO_4 solution (10 g, 1.0 M) was acidified with HCl (1.0 M) to within the pH range 1.65−1.75. Hydrothermal treatment (155 °C, 30−48 h) of the resultant solution was undertaken in Teflon-lined Parr acid digestion bombs to afford a pale green solid which was washed with deionized water until the pH of the eluant was neutral, and dried to constant weight at 75 °C in air. The preparation of variably molybdenum-doped phases (Mo_y-HTB; y = attempted Mo atom % substitution level) was undertaken by adding the required quantity of Na_2MoO_4 solution (1.0 M) to the Na_2WO_4 solution prior to acidification and hydrothermal treatment.

Characterization. Powder X-ray diffraction patterns of the HTB and Mo_y−HTB phases were collected on a Scintag X1 diffractometer in the range 5−80° (2θ), employing Cu Kα radiation (1.542 Å) and a Peltier detector. Elemental analysis of materials was undertaken by energy dispersive spectroscopy (EDS) coupled to either a JEOL 6400m scanning electron microscope or a FXII JEOL transmission electron microscope. Sodium-23 solid-state nuclear magnetic resonance (NMR) spectra of samples at ambient temperature were acquired on a Bruker MSL400 spectrometer operating at 105.805 MHz and 15 kHz MAS frequency. Data were processed using the WINNMR software. Thermogravimetric analyses (TGA) and differential thermal analsyses (DTA) were conducted simultaneously on a Setaram TAG24 (France). Elemental analysis of cation-containing acidic solutions were performed using inductively coupled plasma mass spectrometry (ICPMS).

Ion Exchange Investigations. The ion-exchange behavior of sorbents was investigated using the batch contact method. Typically for equilibrium batch contact data, powdered sorbent (200 mg) and a given aqueous cation solution (20 mL) were contacted at 25 °C for 24 h with constant agitation after which time the supernatant was removed and filtered (0.45 μm), and equilibrium metal cation concentrations were analyzed by ICPMS. Specific solution concentrations of metal species are given in the captions of the figures. Determination of the metal cation concentrations before and after contact with a given sorbent allows the calculation of a distribution coefficient (K_d) for the given metal cation with respect to the sorbent by the formula

$$K_d = \frac{(C_i - C_f)}{C_f} \cdot \frac{V}{mF} \quad (1)$$

where C_i = initial cation concentration; C_f = final cation concentration; V = volume of solution contacted with sorbent; m = mass of sorbent employed; and F = form factor to normalize for hydration of the given sorbent, or in other words the fraction of dried material in the sample. All batch contact experiments were conducted using $V/m = 100$ mL·g^{-1} to allow direct comparison of results.

Results and Discussion

Initial determinations of Cs^+ and Sr^{2+} ion-exchange selectivities (K_d) for the undoped HTB and PYRO phases from acidic solutions were conducted alongside a range of undoped and Nb-doped silicotitanates (Nb−SiTi) having the sitinakite structure. The sorbents were contacted with ANSTO (Australian Nuclear Science and Technology Organization) intermediate-level liquid waste (ILLW) simulant (see caption of Table 1) and the Cs^+ and Sr^{2+} selectivity data observed are presented in Table 1. This simulant solution has a somewhat simpler composition than the ^{137}Cs- and ^{90}Sr-containing ILLW originating from radiopharmeutical production at the ANSTO site which includes parts-per-million concentrations of Al^{3+}, Mg^{2+}, Na^+, and Fe^{3+}, and 1−900 MBq·L^{-1} of numerous fission products in ca. 0.8 M HNO_3. Also included in Table 1 for comparison are Cs^+ and Sr^{2+} distribution coefficients, measured with the same simulant, for HTB synthesized using 1.0 M HNO_3 in place of 1.0 M HCl; AMP/PANsf (0.3−0.6 mm bead size) composite absorber; and a number of antimony silicates doped to varying degrees with silicon.

Table 1. Distribution Coefficient (K_d) Values for Powdered Inorganic Ion-Exchangers Measured Using ANSTO ILLW Radwaste Simulant (2.0 ppm Cs; 0.6 ppm Sr; 1.0 M HNO_3)

sample	Cs K_d(mL·g^{-1})	Sr K_d(mL·g^{-1})
Nb−SiTi	8050	0
Nb_x−SiTi ($x = 0.1$)	16200	0
Nb_x−SiTi ($x = 0.2$)	8050	12
Nb_x−SiTi ($x = 0.3$)	3980	6
PYRO	5870	20
HTB	39900	2300
HTB (HNO_3)	30900	2600
AMP/PANsf (85.7%w/w)	17600	0
$SbSi_x$−PYRO ($x = 0.0$)	36	20400
$SbSi_x$−PYRO ($x = 0.05$)	166	23360
$SbSi_x$−PYRO ($x = 0.10$)	205	21900

These data make it apparent that while the sitinakite-based silicotitanates, PYRO, and AMP/PANsf materials are quite selective for Cs^+ under these acid conditions, they have little if any selectivity for Sr^{2+}. For the sitinakite-based materials and AMP/PANsf absorber, this behavior has been reported previously.[21,23,24] The antimony silicate materials display the highest selectivity for Sr^{2+} of all the materials investigated under these conditions, but as expected from previous reports,[8,10,25] they show significantly less selectivity for Cs^+. Interestingly, both the HTB variants display Cs^+ selectivity comparable to that of the optimized Nb^{5+}-doped silicotitanate ($x = 0.1$) and AMP/PANsf but in addition display good selectivity for Sr^{2+}. In essence, the structural sites within the HTB framework involved in ion-exchange must possess a strong preference for both Cs^+ and Sr^+ over hydronium ions. This preference for Cs^+ and Sr^{2+} cations under these conditions appears directly linked to the ionic radii of the cations (Cs^+ 1.67 Å; Sr^{2+} 1.18 Å). Although this is almost certainly an oversimplification of the actual basis of selectivity, it would seem appropriate given that comparable or increased selectivities (w.r.t. hydronium ions) have been observed for cations with similar ionic radii such as Ag^+ (1.15 Å), Pb^{2+} (1.19 Å), and Tl^+ (1.59 Å) (Figure 2). The ion-exchange properties of the HTB system with respect to each of these cations is currently being investigated for a range of separation-based applications.

(21) Poojary, D. M.; Cahill, R. A.; Clearfield, A. *Chem. Mater.* **1994**, *6*, 2364.
(22) Luca, V.; Hanna, J. V.; Smith, M. E.; James, M.; Mitchell, D. R. G.; Bartlett, J. R. *Microporous Mesoporous Mater.* **2002**, *55*, 1.
(23) Todd, T. A.; Mann, N. R.; Tranter, T. J.; Sebesta, F.; John, J.; Motl, A. *J. Radioanal. Nucl. Chem.* **2002**, *254*, 47.
(24) Todd, T. A.; Brewer, K. N.; Wood, D. J.; Tullock, P. A.; Mann, N. R.; Olson, L. G. *Sep. Sci. Technol.* **2001**, *36*, 999.
(25) Harjula, R. O.; Moller, J. T.; Amin, S.; Dyer, A.; Pillinger, M.; Newton, J. A.; Tusa, E. H.; Webb, M. WO Patent 9959161, 1999.

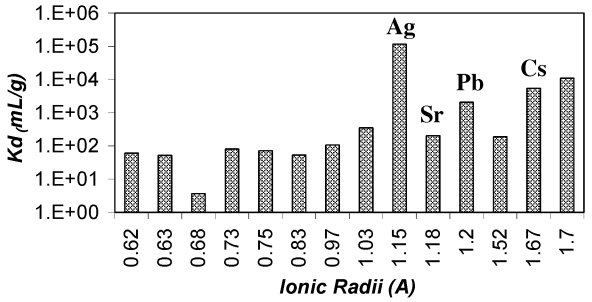

Figure 2. Selectivity of $Mo_{0.1}$−HTB phase for various cations (100 ppm) in 1.0 M HNO_3. Ionic radii taken from compilation of Liebau[31] which uses values from Shannon.[32−34]

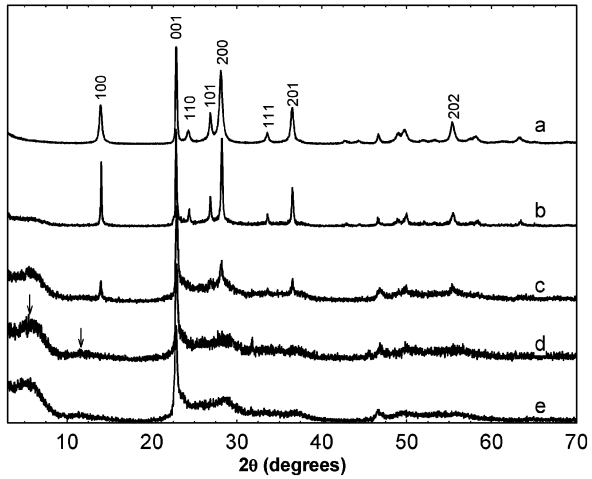

Figure 3. Powder X-ray diffraction patterns of HTB phases with attempted composition $Na_{0.2}Mo_yW_{1-y}O_3{\cdot}ZH_2O$ ($y = 0$, 0.05, 0.10, 0.15, 0.20 in a, b, c, d, e, respectively). Arrows indicate additional unexplained broad reflections. Miller indexes are included for the major reflections only.

The encouraging selectivity of the HTB system for *both* Cs^+ and Sr^{2+} indicates potential scope for improving the ion exchange properties, especially with respect to Sr^{2+}. One strategy for modulating the cation selectivity is the insertion of heteroatoms into the framework W^{6+} sites thereby possibly affecting channel dimensionality and acidity of the ion exchange sites. Perhaps one of the most obvious candidates for this isomorphous substitution is Mo^{6+} which has only a slightly smaller ionic radius (0.59 Å) than W^{6+} (0.60 Å) and exhibits solution chemistry similar to that of W^{6+}.[26] This similarity in solution chemistry between molybdenum and tungsten significantly simplifies the synthesis of monophasic materials.[27]

The X-ray diffraction (XRD) patterns of the resultant materials with attempted $Na_{0.2}Mo_yW_{1-y}O_3{\cdot}ZH_2O$ compositions (Mo_y−HTB; $y = 0$, 0.05, 0.10, 0.15, 0.20) are shown in Figure 3 (a, b, c, d, and e, respectively). The pattern of the phase with $y = 0$ matches very well that reported previously and can be refined by Rietveld techniques in the space group $P6mmm$. For $y = 0.05$, a narrowing of all of the HTB reflections occurs and Rietveld refinements indicate that measurable changes occur in the lattice parameters. When $y = 0.10$, the characteristic HTB reflections are still observed, with little difference in the measured line widths in comparison to the $y = 0.05$ sample. However, the narrow reflections are diminished in intensity relative to the background, and several weak and broad reflections are observed at low angles. The crystallinity clearly continues to degrade as more molybdenum is added to each synthesis. Concomitantly, the low angle feature first observed at ca. 5.8° (2θ) in the pattern of the $y = 0.05$ sample moves to even lower diffraction angles and its relative intensity diminishes. Similar observations have been made where other metal dopants (Ti^{4+}, Zr^{4+}, Nb^{5+}) have been employed.[27]

On the basis of the XRD data alone, these observations could be explained by the presence of an additional phase, loss of long range order, or defects in the hexagonal structure. To clarify this point, the parent HTB and $Mo_{0.1}$−HTB phases were subjected to detailed scanning transmission electron microscopy (STEM) investigations. Whereas the HTB phase consists of single particles with fibrous morphology of relatively uniform thickness, but varying length (Figure 4), the same cannot be said for the $Mo_{0.1}$−HTB phase (Figure 5).

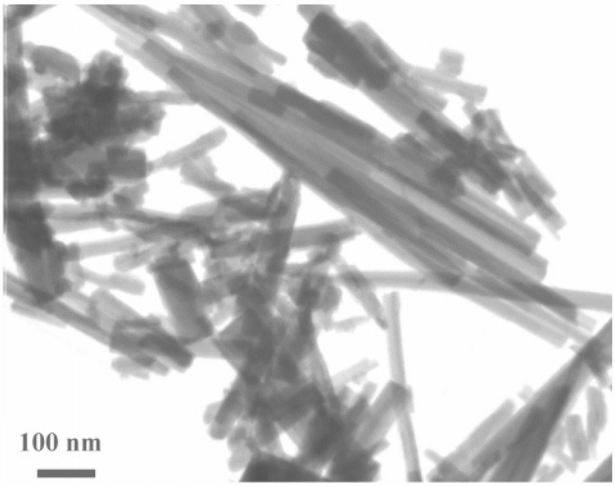

Figure 4. STEM micrograph of the as-synthesized HTB sample.

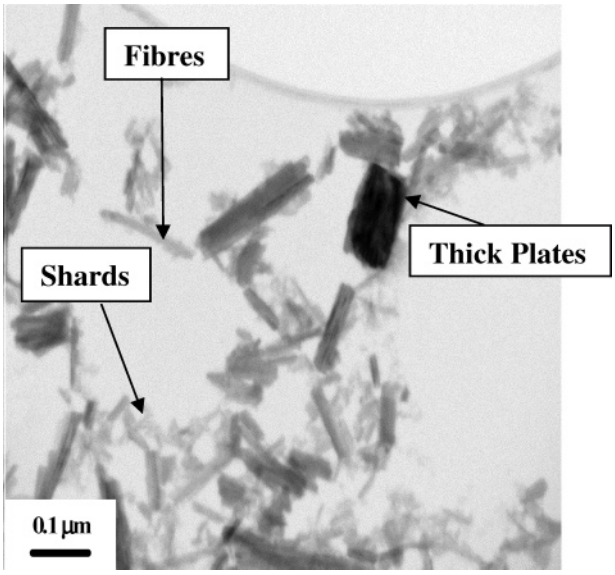

Figure 5. STEM micrograph showing the three morphologies observed in the as-synthesized $Mo_{0.1}$−HTB sample.

(26) Cotton, F. A.; Wilkinson, G. *Advanced Inorganic Chemistry*, 5th ed.; Wiley-Interscience: New York, 1988.
(27) Luca, V. WO Patent 0296559, 2002.

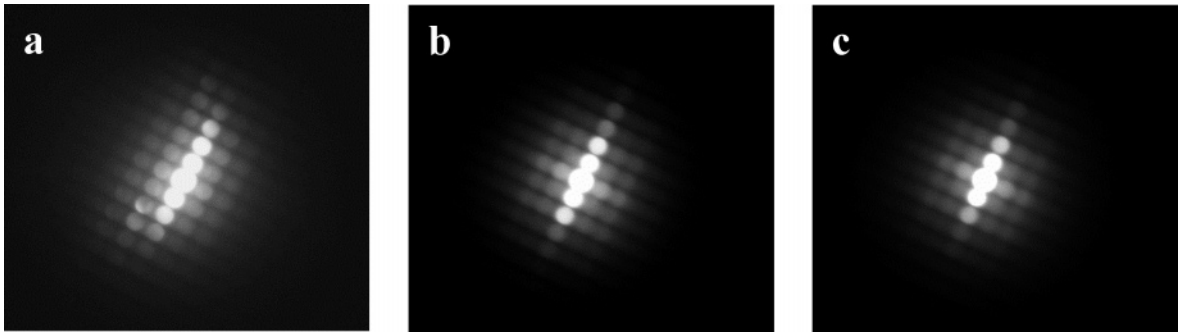

Figure 6. Selected area electron diffraction patterns of $Mo_{0.1}$−HTB: a = fiber; b = shard; c = thick plate.

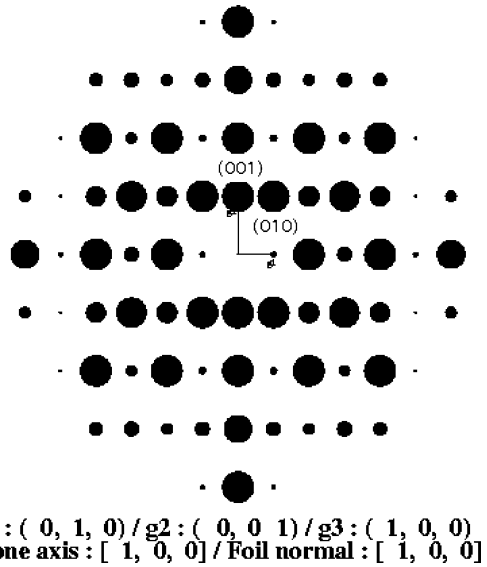

Figure 7. Theoretical electron diffraction pattern for the *P6mmm* space group.

Generally, the $Mo_{0.1}$−HTB phase contains three types of particle morphologies which can be described as thick plates, fibers, and shards. Low magnification micrographs indicate that the particles with the thick plate morphology are far less numerous than the fibrous particles. Selected area diffraction patterns of all the particle morphologies (Figure 6) are characteristic of the *P6mmm* space group (Figure 7). Surprisingly though, EDS analysis of these particle morphologies, throughout the sample, show that the amount of molybdenum incorporated within the framework of the tungstate phases is about one-third that in the reactant mixture. Hence, for the $Mo_{0.1}$−HTB phase the composition is more consistent with the formula $Na_{0.2}Mo_{0.03}W_{0.97}O_3{\cdot}ZH_2O$. Despite the known similarities in solution chemistry between molybdenum and tungsten, it would appear that the solid-state chemistry of the two is sufficiently different such that the solid-solution limit for molybdenum in the HTB phase is quite low. Presumably, the excess molybdenum remains in the solution phase of the reaction mixture as no molybdenum-rich phases are observed in these samples.

To determine whether the multiple particle morphologies drastically affect the overall ion-exchange performance, the selectivities of the three particle morphologies for Cs^+ were investigated by saturating a portion of the $Mo_{0.1}$−HTB sample with 50 mM Cs^+ in 1.0 M HNO_3. Micrographs of this material are comparable to that observed for the parent $Mo_{0.1}$−HTB sample (Figure 5), showing no morphological changes or changes to the *P6mmm* symmetry on Cs^+ incorporation, as judged by the selected area electron diffraction patterns (Figure 8). The EDS analyses from this Cs^+-saturated material show that the Cs^+ atom % of the fibers and shards are consistently higher than that of the thick plate morphology particles. This may be a result of substantially reduced ion-exchange kinetics in the larger particles, but given the relatively small percentage of such particles, it has been concluded that this should not drastically reduce the Cs^+ selectivity or uptake on a unit weight basis. Additionally, EDS analyses appear to indicate that Cs^+-exchange effectively removes all of the Na^+ from all three morphologies. However, ^{23}Na solid-state NMR investigations clearly show that a small proportion of Na^+ remains bound within the tungstate framework. The position and coordination environment of these nonexchangeable sodium cations within the framework are the subject of ongoing investigations.

The impact of variable molybdenum-doping of the HTB framework on Cs^+ and Sr^{2+} selectivity is presented in Figure 9. For each attempted composition with increased molybdenum-doping, a concomitant increase in Cs^+ and Sr^{2+} selectivity, with respect to the parent HTB phase, is observed. The optimum substitution level is observed at the attempted 10 atom % level ($Mo_{0.1}$−HTB), which results in a not insignificant 5-fold increase in distribution coefficient for both Cs^+ and Sr^{2+} and an improvement in capacity.

In addition to the high selectivity of the tungstate phases for Cs^+ and Sr^{2+}, the time dependence of the ion-exchange mechanism is also of prime importance. Investigations conducted using batch contact experiments reveal that for both the parent HTB and optimized $Mo_{0.1}$−HTB phases, maximum sorption of Cs^+ (Figure 10) and Sr^{2+} (Figure 11) occurs after only 30−60 min of contact. These rapid kinetics demonstrate that ion-exchange is not affected by the crystalline nature of the phase. Furthermore, the results demonstrate that the 24 h contact time protocol employed is sufficient to establish equilibrium.

The drying temperature employed after hydrothermal preparation of the tungstate phase impacts significantly upon the Cs^+ and Sr^{2+}-sorption performance of these materials. For samples dried at 75 °C, consistent distribution coefficients for Cs^+ and Sr^{2+} are observed with acidic solutions (1.0 M HNO_3) containing Cs^+ (2.0−100 ppm) and Sr^{2+} (0.6−60 ppm). However, for samples heated between 100 and 500 °C extreme changes in the Cs^+ and Sr^{2+} distribution coefficients are observed (Figure 12).

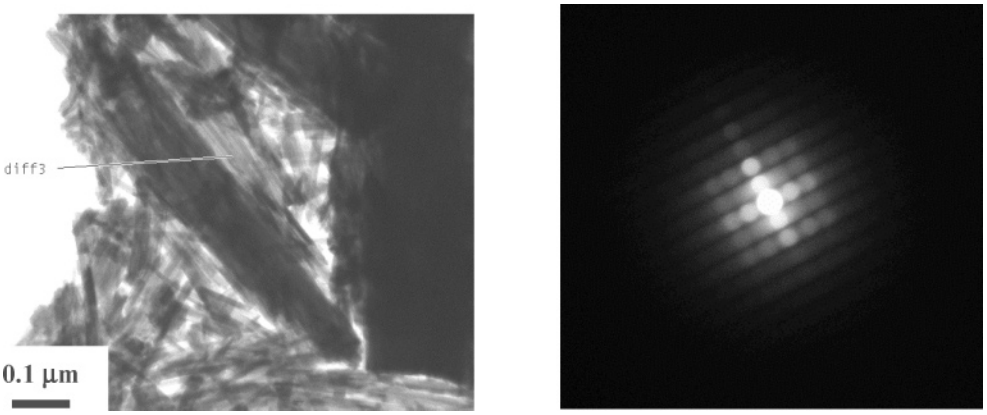

Figure 8. Selected STEM micrograph of Cs-saturated ($Cs_{0.26}$) $Mo_{0.1}$−HTB sample (left) and selected area electron diffraction pattern (right).

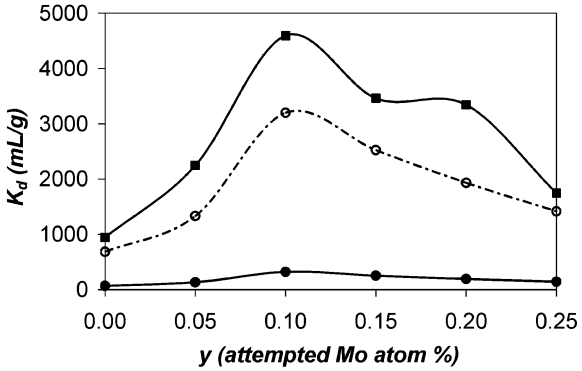

Figure 9. Selectivity of Mo_y−HTB phases as a function of *y* (attempted Mo atom %) measured with solutions comprising 100 ppm Cs (-■-) or 66 ppm Sr (-●-) and 200 ppm Na, 1.0 M HNO_3. Scaled (×10) Sr^{2+} selectivity (-○-).

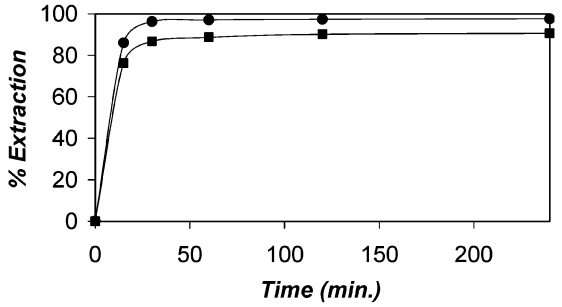

Figure 10. Time-dependent uptake of Cs^+ by HTB (-■-) and $Mo_{0.1}$−HTB (-●-) from solutions comprising 160 ppm Cs, 96 ppm Sr, 200 ppm Na, 1.0 M HNO_3.

During the calculation of the distribution coefficient, the level of hydration for a given sorbent can be factored into the equation to normalize results for "pure" non-hydrated sorbent (eq 1). A comparison of the original (Cs^+ -■-; Sr^{2+} -●-) and normalized distribution coefficients (Cs^+ -□-; Sr^{2+} -○-) is presented in Figure 12 and clearly shows that this factor alone is not responsible for the increases in Cs^+ and Sr^{2+} selectivity. We are currently probing subtle changes in the tungstate framework in this temperature regime with X-ray, synchrotron, neutron diffraction, and solid-state NMR techniques, with a view to better understanding this phenomena. However, initial investigations show that the unit cell of the tungstate sorbents measurably constricts along the *c*-axis when heated in the region 75−300 °C.

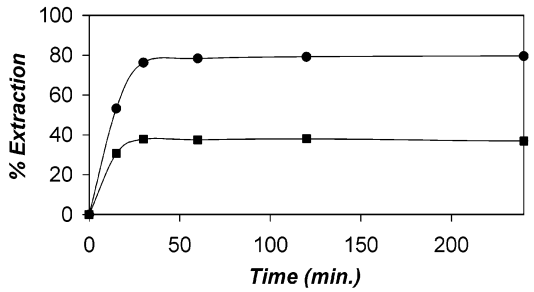

Figure 11. Time-dependent uptake of Sr^+ by HTB (-■-) and $Mo_{0.1}$−HTB (-●-) from solutions comprising 160 ppm Cs, 96 ppm Sr, 200 ppm Na, 1.0 M HNO_3.

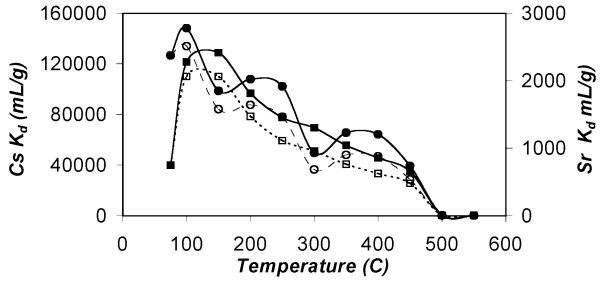

Figure 12. Dependence of the Cs^+ (-■- and -□-, unnormalized and normalized for dehydration, respectively) and Sr^{2+} (-●- and -○-, unnormalized and normalized for dehydration, respectively) distribution coefficients ($mL \cdot g^{-1}$) upon sorbent drying temperature; 2 ppm Cs^+, 0.5 ppm Sr^{2+}, 10 ppm Na^+, 1.0 M HNO_3.

Another important property of any ion-exchanger is its capacity for a given ionic species. The HTB and $Mo_{0.1}$−HTB phases possess a *theoretical* maximum A cation content corresponding to the formula, $A_{0.3}WO_3 \cdot H_2O$, which in turn corresponds to a theoretical capacity of 0.9 $mmol \cdot g^{-1}$ for monovalent cations such as Cs^+.[20] Our investigations with the HTB phase have revealed that with a 1000-fold excess of either Cs^+ or Sr^{2+} in 1.0 M HNO_3, capacities of only 0.2 and 0.12 $mmol \cdot g^{-1}$, respectively, are consistently observed. For the $Mo_{0.1}$−HTB phase, the Cs^+ and Sr^{2+} equilibrium isotherm curves are presented in Figure 13. The solid lines represent Langmuir fits to the experimental data. The calculated cation exchange capacity (CEC) and q_o ("capacity") for Cs^+ and Sr^{2+} are 0.444 $mmol \cdot g^{-1}$ (59 $g \cdot kg^{-1}$) and 0.252 $mmol \cdot g^{-1}$ (22.1 $g \cdot kg^{-1}$), respectively, and are ca. 50% of the theoretical CEC implied by the ideal $A_{0.3}WO_3 \cdot H_2O$ formulas. Comparison of the Cs^+ CEC of

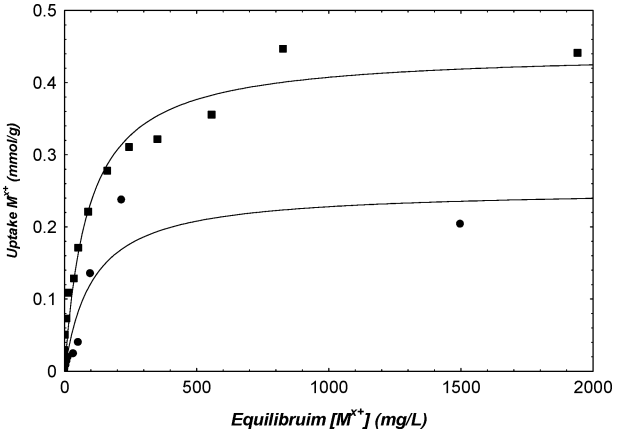

Figure 13. Equilibrium Cs^+ (-■-) and Sr^{2+} (-□-) Langmuir isotherms for $Mo_{0.1}$−HTB adsorbent. Cs^+ − k = 0.0113; q_o = 0.444 mmol·g^{-1}; r^2 = 0.96. Sr^{2+} − k = 0.0094; q_o = 0.252 mmol·g^{-1}; r^2 = 0.899.

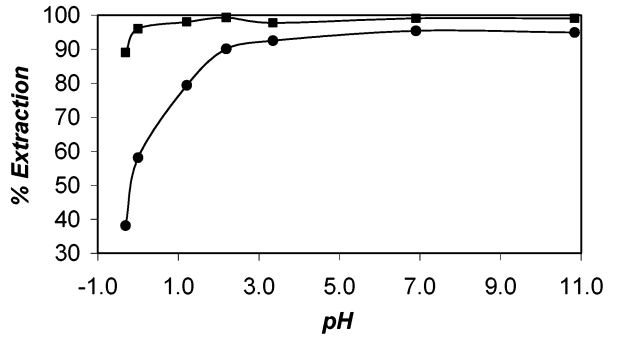

Figure 14. pH-dependence of Cs^+ (-■-) and Sr^{2+} (-●-) extraction efficiency (selectivity) for $Mo_{0.1}$−HTB phase; 100 ppm Cs^+, 66 ppm Sr^{2+}, 10 ppm Na^+.

both the HTB and $Mo_{0.1}$−HTB phases with ammonium molybdophosphate (0.6 mmol·g^{-1}; 85 g·kg^{-1}) [28] shows that the CEC for Cs^+ of the HTB-based absorbents is significantly lower. Furthermore, it has been surmised that the residual Na^+ within the HTB framework, as indicated by the ^{23}Na solid-state NMR data, must contribute to the lower than theoretical CEC of the HTB and $Mo_{0.1}$−HTB phases.

The plot in Figure 14 outlines the Cs^+ and Sr^{2+}-extraction efficiency of $Mo_{0.1}$−HTB as a function of simulant pH. For Cs^+ (-■-) the percentage extraction does not vary greatly across the H_3O^+ range studied, except at low pH where a decrease to 87% extraction is observed. It should be noted that even at exceptionally low pH (6.0 M HNO_3), extraction of 20% of Cs^+ is still observed with 100 ppm solutions. This is especially impressive as few conventional inorganic adsorbents can tolerate such acidity without decomposition. The lower selectivity of the $Mo_{0.1}$−HTB phase for Sr^{2+} (-●-) is clearly evident from the plot in Figure 14, with maximum Sr^{2+} extraction observed only under neutral conditions. As the pHs of the given simulants are decreased below 2.1 to −0.3, the Sr^{2+} extraction decreases from 90% to 38% extraction.

The extraction efficiency of the $Mo_{0.1}$−HTB phase outlined in Figure 14 only demonstrates the selectivity of the phase in competition with H_3O^+. With reference

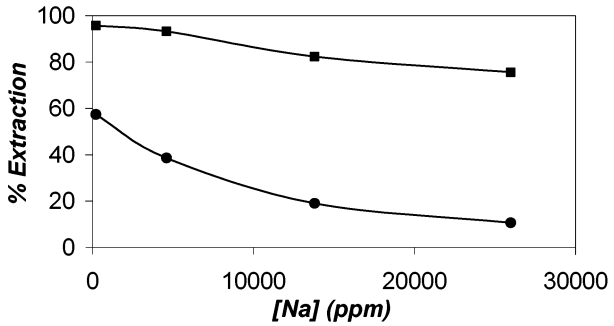

Figure 15. Dependence of Cs^+ (-■-) and Sr^{2+} (-●-) extraction efficiencies (selectivity) for the $Mo_{0.1}$−HTB phase from acidic solution, as a function of Na^+ concentration; 100 ppm Cs^+, 66 ppm Sr^{2+}, 1.0 M HNO_3.

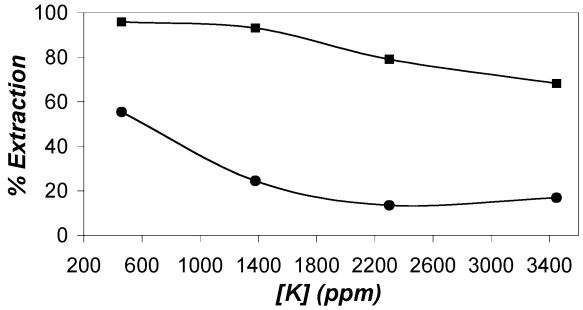

Figure 16. Dependence of Cs^+ (-■-) and Sr^{2+} (-●-) extraction efficiency (selectivity) for the $Mo_{0.1}$−HTB phase from acidic solution, as a function of K^+ concentration; 100 ppm Cs^+, 66 ppm Sr^{2+}, 1.0 M HNO_3.

to the ILLW produced at the ANSTO site, selectivity of a given sorbent versus H_3O^+ is the major concern in assessing its applicability to pretreatment of this radwaste due to its relatively simple nature. However, given that several ^{137}Cs- and ^{90}Sr-containing radwaste streams throughout the world contain high levels of Na^+, K^+, and also Ca^{2+}, the effect that various levels of these common competing cations have on the performance of the $Mo_{0.1}$−HTB phase is also of particular interest.

The plot in Figure 15 shows the Cs^+ and Sr^{2+} distribution coefficients for the $Mo_{0.1}$−HTB phase as a function of Na^+ cation concentration from 1.0 M HNO_3 solutions. The inclusion of a moderate level of Na^+ (5000 ppm) can be seen to have an immediate negative impact on Sr^{2+} sorption, decreasing ca. 20% to 38% extraction, whereas Cs^+ sorption is relatively unaffected. In fact, the extraction of Cs^+ remains above 80% up to 14 000 ppm Na^+, and through to 25 000 ppm, only reduces a further 7%. In contrast, Sr^{2+} sorption over the same region decreases to 10%. Similar results are observed with increasing K^+ cation concentration (Figure 16) but the decreases in extraction of Cs^+ and Sr^{2+} occur at much lower concentrations. The plot in Figure 17 shows the Cs^+ and Sr^{2+} distribution coefficients for the $Mo_{0.1}$−HTB phase as a function of Ca^{2+} cation concentration from 1.0 M HNO_3 solutions. The results show that even modest levels of Ca^{2+} (100−1000 ppm) drastically decrease Sr^{2+} extraction. The effect is so pronounced that above 5000 ppm Ca^{2+}, less than 10% extraction is observed. As observed for increasing levels of Na^+ and K^+, increasing levels of Ca^{2+} do not drastically impact the extraction of Cs^+, with an almost linear

(28) Tranter, T. J.; Herbst, R. S.; Todd, T. A.; Olson, A. L.; Eldredge, H. B. *Adv. Environ. Res.* **2002**, *6*, 107.

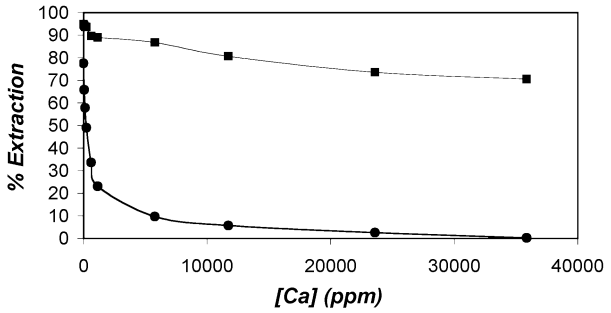

Figure 17. Dependence of Cs^+ (-■-) and Sr^{2+} (-●-) extraction efficiency (selectivity) for the $Mo_{0.1}$−HTB phase from acidic solution, as a function of Ca^{2+} concentration; 100 ppm Cs^+, 66 ppm Sr^{2+}, 1.0 M HNO_3.

decrease from 89% extraction at 1000 ppm Ca^{2+} through to 70% extraction at ca. 36 000 ppm Ca^{2+}.

The greater effect on Sr^{2+} selectivity, as compared to that for Cs^+, observed in the presence of K^+, Ca^{2+}, and Na^+ implies that these cations are preferentially sorbed by the $Mo_{0.1}$−HTB ion-exchange sites which also sorb Sr^{2+}. We have rationalized these observations on the basis that the ionic radii of the bare cations (1.38, 1.00, and 1.02 Å, respectively) are comparable with that of Sr^{2+} (1.18 Å).

In the context of potentially applying the optimized $Mo_{0.1}$−HTB sorbent to the pretreatment of liquid radwaste containing significant levels of Na^+, K^+, and Ca^{2+}, such as the "sodium-bearing" waste at the Idaho Nuclear Technology and Engineering Center (INTEC),[29] these results indicate that only moderate levels of ^{137}Cs, and little to no ^{90}Sr, would be removed from this particular liquid radwaste stream.

Conclusions

The ability of HTB-based phases to effectively sorb both Cs^+ and Sr^{2+} from highly acidic solutions represents a major advantage over inorganic ion-exchangers such as AMP/PANsf and $Na_2Ti_{2-x}Nb_xO_3SiO_4{\cdot}2H_2O$, which are known to only sorb Cs^+ under acidic conditions. The Nb-doped antimonates might compete with the present materials in this respect but a proper comparison would require testing of selectivity, capacity, stability, and kinetics of the two materials under identical experimental conditions.

While research to date indicates that the selectivity of microporous inorganic materials for a particular cationic species is largely dependent on the geometry of the structural sites,[30] other factors such as surface acidity, water structure in the channel, and electronegativity may also influence selectivity. This makes the situation somewhat more complicated. In the materials being considered here we have found the peculiar situation of enhanced selectivity for cations having ionic radii of approximately 1.2 and 1.7 Å. Owing to the inherent disordered nature of HTB materials even when they do not contain framework dopants, it is expected to be extremely difficult to deduce the siting of both cations in the structure using diffraction or other techniques. One possibility is to try to improve crystallinity of materials that are saturated in both Cs^+ and Sr^{2+} by calcinations in air and this may make it possible to better locate cation positions. However, this would require operating under the assumption that dehydration of the materials does not result in movement of the cation sites occupied on ion exchange.

While the initial investigations reported herein appear to indicate that the molybdenum-doped HTB phase, $Mo_{0.1}$−HTB, displays sorption performance conducive to the pretreatment of the ^{137}Cs- and ^{90}Sr-containing ILLW at the ANSTO site, application to other acidic radwaste streams with significant levels (>5000 ppm) of Na^+, K^+, or Ca^{2+}, appears unlikely.

Successful modulation of Cs^+ and Sr^{2+} selectivity for the HTB phase by simple molybdenum-doping suggests that other metal dopants, which are capable of imparting greater dimensional changes to the channels of the HTB framework, might offer further improvements in selectivity for these two cations, or other environmentally relevant cations.

Acknowledgment. Contributions to sorbent preparation, optimization, and testing by Harriet Chronis and Jonathon Widjaja are gratefully acknowledged. ICPMS analysis by Jim Foy and Nicholas Scales has been invaluable, along with STEM and electron diffraction data collected by Dr Huijun Li. The acquisition of ^{23}Na solid-state NMR spectra by John Hanna is also gratefully acknowledged.

CM049335W

(29) Herbst, R. S.; Law, J. D.; Todd, T. A. *Sep. Sci. Technol.* **2002**, *37*, 1321.

(30) Tripathi, A.; Medvedev, D. G.; Nyman, M.; Clearfield, A. *J. Solid State Chem.* **2003**, *175*, 72.

(31) Liebau, F. *Structural Chemistry of Silicates: Structure, Bonding, and Classification*; Springer-Verlag: Berlin, 1985; p 347.

(32) Shannon, R. D. *Acta Crystallogr., Sect. A: Cryst. Phys., Diffr., Theor. Gen. Crystallogr.* **1976**, *A32*, 751.

(33) Shannon, R. D.; Prewitt, C. T. *Acta Crystallogr., Sect. B: Struct. Crystallogr. Cryst. Chem.* **1969**, *25*, 925.

(34) Shannon, R. D.; Prewitt, C. T. *Acta Crystallogr., Sect. B: Struct. Crystallogr. Cryst. Chem.* **1970**, *26*, 1046.